Kinetic Study of the Hydrogenation and Hydroisomerization of the *n*-Butenes on a Commercial Palladium/Alumina Catalyst

Sergio P. Bressa, Osvaldo M. Martínez, and Guillermo F. Barreto*

Centro de Investigación y Desarrollo en Procesos Catalíticos (CINDECA) and Proyecto de Investigación y Desarrollo en Ingeniería de Reactores Químicos (PROIRQ), Universidad Nacional de La Plata, C.C. 59, B1900AJK - La Plata, Argentina

A kinetic investigation of the vapor-phase hydrogenation and hydroisomerization of 1-butene and *cis*- and *trans*-2-butene is presented. This investigation is aimed at validating a practical set of rate equations. The experiments were performed at approximately atmospheric pressure using a commercial Pd/Al_2O_3 catalyst of the eggshell type in an integral fixed-bed isothermal reactor. The outlet composition was measured under 120 sets of operating conditions at six levels of temperature between −8 and 30 °C. The mole fractions of 1-butene and hydrogen in the feed were varied between 0.5 and 3% and between 0.5 and 50%, respectively. Space-time covered the range of $(5-55) \times 10^{-3}$ s. Internal diffusion limitations affected the effective reaction rates and product distribution. Hence, the mass conservation equations inside the catalyst had to be solved to estimate the intrinsic values of the kinetic parameters. Two rival kinetic models of the Langmuir−Hinshelwood−Hougen−Watson type were proposed, one of which could be confidently discriminated as the better of the two models considered. An essential feature of the chosen model is that hydrogen concentration exhibits distinct effects on the hydrogenation and hydroisomerization reactions of *n*-butenes. The selected model predicts the experimental results with an average deviation of 8.8%. The estimates of the kinetic parameters show inference intervals in the range of ±10−30%.

Introduction

The sources of unsaturated C_4 cuts are streams from cracking operations. Selective hydrotreatment is the proper method for upgrading these C_4 cuts. The selective hydrogenation of 1,3-butadiene to 1-butene and the selective hydroisomerization of 1-butene to 2-butenes are examples of the hydrorefining of *n*-butenes-rich cuts.[1] These processes involve the hydrogenation and hydroisomerization of the *n*-butenes. We expect the kinetic study proposed in this work to provide valuable information on factors that affect the selectivity of hydrorefining processes, such as catalyst features and operating conditions of industrial reactors.

Bond and Wells[2] and Webb[3] previously discussed product distribution patterns, possible mechanisms, and other relevant kinetic trends concerning the reactions of *n*-butenes over Pd catalysts. Boitiaux et al.[4] proposed a kinetic model for the hydrogenation and irreversible isomerization of 1-butene. Their model is based on qualitative information obtained from the liquid-phase reaction of 1-butene over a laboratory Pd/Al_2O_3 catalyst. Vergel et al.[5] calculated the ratios between the kinetic coefficients of the hydrogenation and isomerization reactions of 1-butene according to the model proposed by Boitiaux et al.[4] The experiments were performed in the liquid phase at 40 °C on a commercial Pd/Al_2O_3 catalyst of the eggshell type. However, the work of Vergel et al.[5] was not aimed at a kinetic study. Goetz et al.[6] studied the vapor-phase reactions of 1,3-butadiene and *n*-butenes at 0 °C over an experimental Pd/γ-Al_2O_3 catalyst. They developed a kinetic model based on a catalytic mechanism and estimated relations between kinetic coefficients rather than their individual values. The experimental data were collected at a constant hydrogen/hydrocarbon ratio. Thus, an insight to some kinetic features could not be assessed.

We conclude that, despite the fair understanding of this system, the validation of a set of practical rate equations remains to be done. The chief target of this work is to present a kinetic model that describes the hydrogenation and hydroisomerization of 1-butene and *cis*- and *trans*-2-butene. The experiments designed to validate the model explored a wide range of composition at six levels of temperature between −8 and 30 °C. The vapor-phase reactions were carried out on a commercial Pd/Al_2O_3 catalyst of the eggshell type.

Experimental Section

Experimental Setup and Materials. Pd-based catalysts are universally used in selective hydrotreatment processes.[1] The main features of the commercial Pd/Al_2O_3 catalyst used in this study are summarized in Table 1.

The kinetic data were obtained in a continuous-flow fixed-bed reactor that consisted of a 3-mm-i.d. tube enclosed in a 15-mm-i.d. jacket operated with a thermostating liquid. The inner tube contained the catalyst bed and inert material.

The first length of the tube was filled with only an inert solid to allow the reacting mixture to attain the desired temperature. Inert Al_2O_3 in a weight ratio of 1:10 was used to dilute the catalyst sample. Both

* To whom correspondence should be addressed. Tel.: + 54 0221 4 21 1353. Fax: + 54 0221 4 25 4277. E-mail: barreto@dalton.quimica.unlp.edu.ar.

10.1021/ie0209879 CCC: $25.00
Published on Web 04/09/2003

Table 1. Catalyst Features

shape	sphere
type	eggshell
diameter	2.5 mm
active layer thickness	2.4×10^{-1} mm
mass fraction of active shell	0.47
Pd loading in the catalyst pellet	0.214 wt %
specific surface area (BET)	71.00 ± 18.26 m^2/g
mean pore radius	36.7 ± 5.5 *n*m
bulk density	1150 kg/m^3
porosity	0.397
specific surface area of Pd	0.55 $m^2/g_{active\ shell}$
metal particle size	3.64 nm
dispersion	27%

catalyst and inert were milled to an average size of 3.35×10^{-1} mm.

A pressure gauge was connected to the reactor inlet to measure the pressure drop. Two thermocouples positioned above and below the catalyst bed indicated the temperature of the reactive mixture.

The experimental system was designed to minimize interparticle gradients and to ensure isothermal and isobaric operation.[7]

1-Butene (99%, Alphagaz), the only hydrocarbon present in the inlet stream, was fed to the reactor after flowing through a guard bed loaded with the same catalyst as used for the tests. H_2 (99.998%, AGA) and N_2 (99.999%, AGA) were purified on a 4A molecular sieve (UOP), followed by an O_2 trap (Alltech).

The commercial catalyst was prereduced, but following standard recommendations, the catalyst samples were exposed in situ to a H_2/N_2 (1:3) stream for 9 h at 54 °C before being used in the tests.

The compositions of the hydrocarbon mixtures fed into and flowing from the reactor were analyzed by gas chromatography. To this end, we employed a 2-m-long 2-mm-i.d. column packed with 0.19% picric acid on 80−100-mesh Graphpac packing at room temperature. In general, three to four chromatographic analyses were made for each set of experimental conditions.

Preliminary Tests. Two blank tests were performed at 30 °C. One of them consisted of feeding 1-butene without hydrogen to the catalyst bed. In the second test, a mixture of 1-butene and H_2 was flowed through a bed of the solid used to dilute the catalyst (Al_2O_3). 1-Butene remained unaltered in both cases, indicating that 1-butene isomerization requires the presence of hydrogen to occur and that the diluting solid was effectively inert.

The results shown in Figure 1 are useful for a discussion of some relevant features concerning the experimental setup and the operating protocol. The exit 1-butene and *n*-butane mole fractions are displayed for different catalyst samples of either 50 or 100 mg, which were the smallest and largest sample sizes employed, respectively. Each catalyst sample, identified by a distinct symbol, was run continuously for about 24−36 h. The pair of values for each catalyst sample in Figure 1 corresponds to the results at the beginning and toward the end of each run. It is clear that the catalyst exhibited a stable activity during the runs.

Figure 1 also makes clear that the exit compositions measured for different samples of the same mass of catalyst exhibits a remarkable constancy. This observation indicates the very good reproducibility level of the experimental protocol and the homogeneity of the catalyst samples.

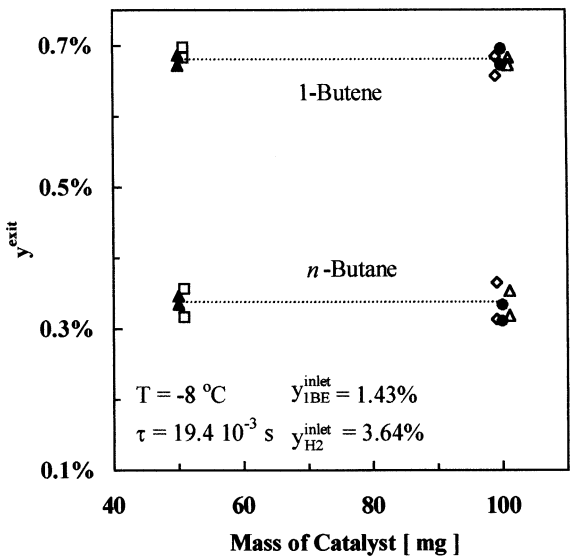

Figure 1. Exit 1-butene and *n*-butane mole fractions for different catalyst samples at the same space-time value and operating conditions. Replicates for two 50-mg catalyst samples are identified by ▲ and □. Replicates for three 100-mg samples are identified by ●, △, and ◇. The pair of values for each catalyst sample corresponds to results at the beginning and end of each experimental run.

The data plotted in Figure 1 correspond to the same value of space-time, τ, i.e., the ratio between the catalyst volume and the volumetric flow rate. To keep τ constant, the flow rate for the 100-mg samples was twice that for the 50-mg samples. No significant difference was observed between the exit compositions in the experiments with 50- and 100-mg samples. This evidence strongly suggests that external mass and temperature gradients were negligible, as was also concluded on the basis of theoretical estimations.[7]

As described in depth by van den Bleek et al.,[8] dilution of the catalyst sample can cause unpredictable behavior when the degree of dilution is high and the ratio between reactor length and particle diameter is low. The smallest catalyst sample, which corresponded to a loading of 50 mg, was checked with the aid of the criteria for avoiding such effects provided by van den Bleek et al.[8] The results with 50- and 100-mg samples in Figure 1, which correspond to the same τ, confirm that dilution effects were negligible.

All aforementioned conclusions were verified for all of the experimental conditions investigated.

Experimental Results

The major trends shown by the experimental results are outlined in this section. They will be used later in this paper to support the proposed kinetic models. The discussion is based on the reaction network sketched in Figure 2.

The set of experimental conditions is summarized in Table 2.

Figure 3a and b shows the dependency of the product composition on the space-time. In this and subsequent figures, the curves correspond to results from the selected model, which will be described later. The distribution of products from the 1-butene reactions can be evaluated at low enough values of τ that the hydrogenation of the 2-butenes has not yet become noticeable. In Figure 3, the experimental data corre-

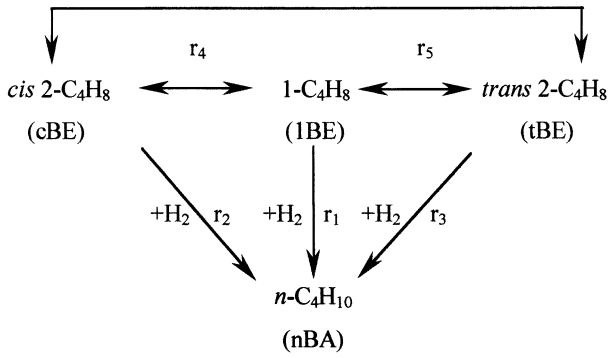

Figure 2. Overall reaction network.

Table 2. Experimental Plan and Settings[a]

temperature (°C)	feed composition y_{1BE}^{inlet} (%)	feed composition $y_{H_2}^{inlet}$ (%)	space-time ($\times 10^{-3}$ s)
−8	0.5−3.0	0.5−50	5−50
0	0.3−2.7	3.6	10.2
5	0.3−2.7	0.5−50	10.1
			18.3
10	0.5−3.0	3.6	9.91
20	0.5−2.7	0.5−20	9.74
			17.3
30	1.4−2.7	3.6	9.48

[a] Catalyst load = 50−100 mg. Volumetric flow rate = 75−300 cm^3/min.

sponding to $\tau < 20 \times 10^{-3}$ s show that the hydrogenation and hydroisomerization of 1-butene take place at similar rates and that *trans*-2-butene is the main isomer produced. The ratio $y_{tBE}^{exit}/y_{cBE}^{exit}$ at low 1-butene conversion decreases slightly with temperature, ranging between 1.5 and 2 within the range of temperatures analyzed. This result agrees with reported data on stereoselectivity.[2]

Figure 3a shows that y_{1BE}^{exit} decreases linearly with increasing τ up to about $(20-25) \times 10^{-3}$ s. This observation suggests that 1-butene consumption follows a zeroth-order rate at high enough concentration. This trend is confirmed by the results in Figure 4, where the difference $(y_{1BE}^{inlet} - y_{1BE}^{exit})$ is nearly constant for values of y_{1BE}^{inlet} greater than about 1.5%. This behavior indicates that 1-butene can saturate the active sites of the catalytic surface. At high values of τ in Figure 3a or low values of y_{1BE}^{inlet} in Figure 4, the mole fraction of 1-butene is lower. Thus, the surface covered by 1-butene decreases, and the apparent reaction order increases.

Figure 5 illustrates that, at higher temperatures, the value of $(y_{1BE}^{inlet} - y_{1BE}^{exit})$ does not remain constant throughout the entire range of y_{1BE}^{inlet}. This result can be explained by the fact that the adsorption of 1-butene is exothermic[9] or also by the possibility that concentration gradients inside the catalyst particles might influence the reaction.

The effect of the hydrogen concentration on the production of *cis*- and *trans*-2-butene from 1-butene at two different temperatures can be observed in Figure 6. A sharp increase in the production rates of both 2-butenes can be observed for low values of $y_{H_2}^{inlet}$. Comparing parts a and b of Figure 6, it can be concluded that temperature exerts a significant effect on the hydrogenation rates of both isomers.

It was verified that, at high enough values of space-time, H_2 input, or temperature, the mole fractions of the *n*-butenes almost reach their thermodynamic equi-

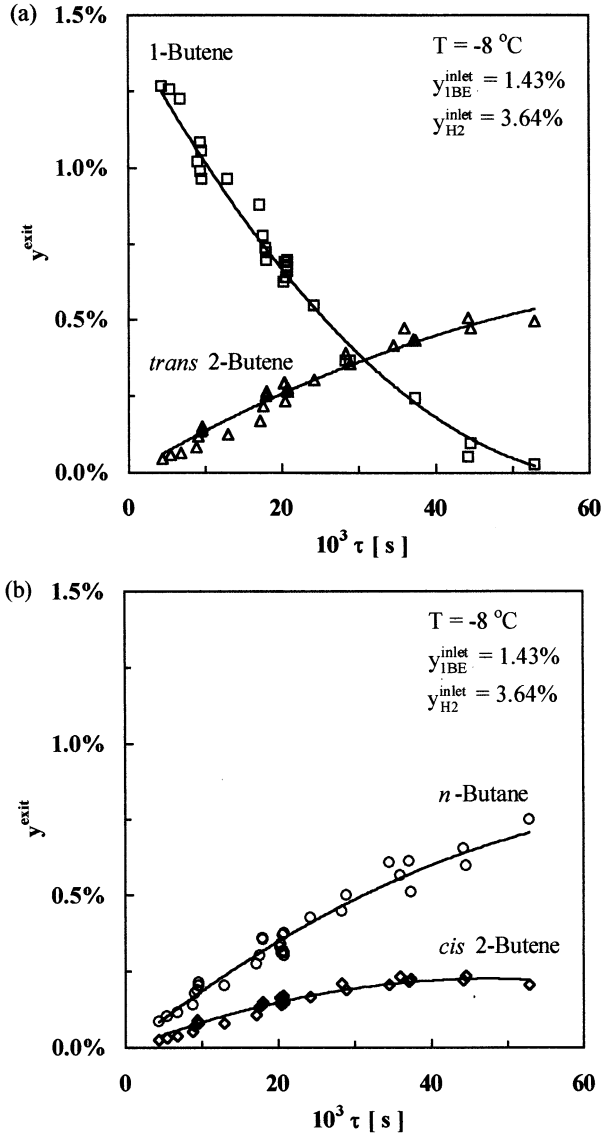

Figure 3. Dependence of product distribution on space-time.

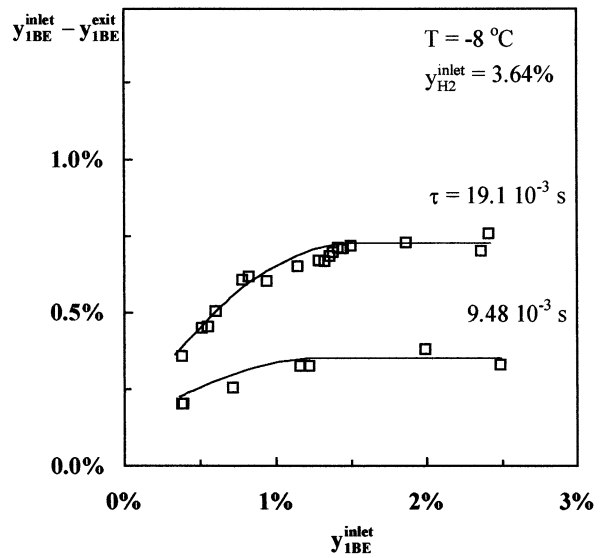

Figure 4. Variation of 1-butene consumption with 1-butene mole fraction in the feed at −8 °C.

librium values. For instance, at 20 °C and $y_{H_2}^{inlet} = 20\%$, the experimental result $y_{1BE}^{exit}/y_{cBE}^{exit}/y_{tBE}^{exit} = 1{:}8{:}23$ is close

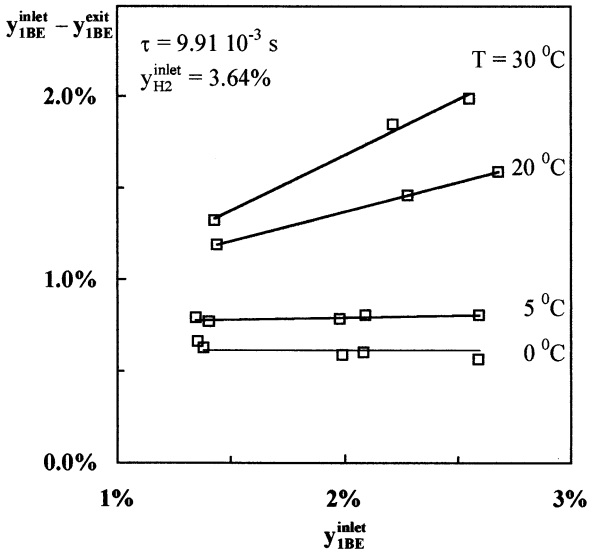

Figure 5. Variation of 1-butene consumption with 1-butene mole fraction in the feed between 0 and 30 °C.

to the equilibrium ratio. This observation called for a consideration of reversible driving forces in the reaction rate expressions developed for the hydroisomerization reactions.

Kinetic Models

Given the fact that the reactions taking place in the studied system are strongly interrelated, the option of proposing empirical expressions for the set of reaction rate expressions was not regarded as a practical approach. Instead, if a sensible catalytic mechanism is proposed, the resulting set of kinetic expressions will naturally incorporate the coupling factors. In accordance with this concept, we next present two alternative mechanisms to support the kinetic models developed.

Catalytic Mechanisms. The two catalytic mechanisms are denoted "A" and "D". First, we will describe mechanism D, which is displayed in Table 3. The description of mechanism D will serve as a basis for detailing the distinctive features of mechanism A.

Dissociative adsorption of H_2, step 1 in Table 3, is assumed to occur on sites of type "◇", which are different from the sites of type "◆" involved in the adsorption of hydrocarbons, steps 2−4. This hypothesis that there is no direct competition between the H_2 and the C_4 hydrocarbons for the same site has been employed by other authors.[6,9,10] We will also analyze the case involving the adsorption of H_2 and hydrocarbons on the same site later in this paper.

The adsorption of the *n*-butenes on sites of type ◆ leads to π-adsorbed olefins, which can react with an adatom, H◇, to form two adsorbed butyl radicals, steps 5−8. Whereas only 1-butene can yield the 1-butyl radical, $C_4^{I}H_9$◆, all three *n*-butenes can produce the 2-butyl radical, $C_4^{II}H_9$◆, steps 6−8. The radical $C_4^{II}H_9$◆ is a common intermediate for cis−trans isomerization and for double bond migration.

The hydrogenation of the *n*-butenes is completed by the addition of a second adatom, H◇, to the radicals $C_4^{I}H_9$◆ and $C_4^{II}H_9$◆, steps 9 and 10. The hydrogenation of 1-butene can follow two routes either through the radical $C_4^{I}H_9$◆ or through $C_4^{II}H_9$◆. Instead, the hydrogenation of the 2-butenes proceeds only through the

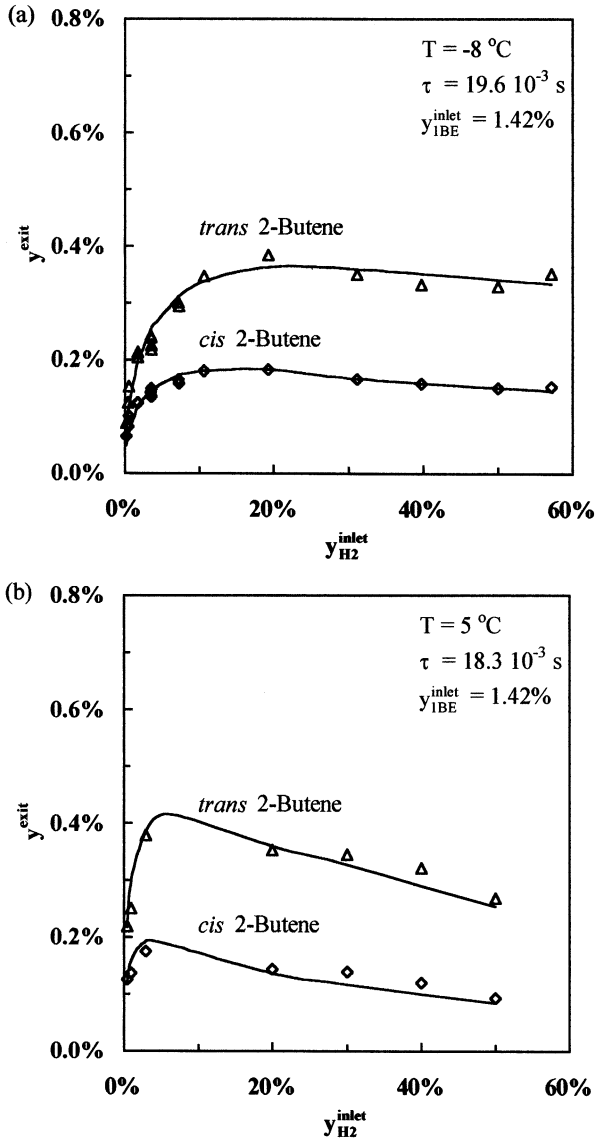

Figure 6. Dependence of 2-butenes production on H_2 mole fraction in the feed at (a) −8 and (b) 5 °C.

radical $C_4^{II}H_9$◆. The formation of *n*-butane is thermodynamically favored and thus considered irreversible. The fraction of active sites occupied by *n*-butane was neglected in view of its weak adsorption.

Essential features of the hydrogenation and hydroisomerization of the *n*-butenes are generally described in terms of the above-mentioned surface hydrocarbon species.[3,6,9,11]

However, the assessment of the source of surface hydrogen is less certain.[2] The hydrogenation of unsaturated hydrocarbons over Pd has been described in terms of two possible hydrogen sources. One source is hydrogen adatoms arising from dissociative adsorption, as in the case of model D.[6,12,13] The other source considered is adsorbed molecules of H_2.[2,9,14,15]

Hence, we decided to include a second mechanism based on the hypothesis that H_2 is adsorbed associatively to produce H_2◇. In this mechanism, called A, the π-adsorbed *n*-butenes react with H_2◇ to form the already described butyl radicals and the surface species H◇ in reactions equivalent to steps 5−8 of Table 3. In turn, the H◇ thus formed is responsible for the final

Table 3. Catalytic Mechanism of Model D

1	$H_2 + 2\diamondsuit \rightleftharpoons 2(H\diamondsuit)$	H_2 adsorption
2	$1BE + \blacklozenge \rightleftharpoons 1BE\blacklozenge$	*n*-butenes adsorption
3	$cBE + \blacklozenge \rightleftharpoons cBE\blacklozenge$	
4	$tBE + \blacklozenge \rightleftharpoons tBE\blacklozenge$	
5	$1BE\blacklozenge + H\diamondsuit \rightleftharpoons C_4^{I}H_9\blacklozenge + \diamondsuit$	formation of the 1-butyl radical
6	$1BE\blacklozenge + H\diamondsuit \rightleftharpoons C_4^{II}H_9\blacklozenge + \diamondsuit$	formation of the 2-butyl radical
7	$cBE\blacklozenge + H\diamondsuit \rightleftharpoons C_4^{II}H_9\blacklozenge + \diamondsuit$	
8	$tBE\blacklozenge + H\diamondsuit \rightleftharpoons C_4^{II}H_9\blacklozenge + \diamondsuit$	
9	$C_4^{I}H_9\blacklozenge + H\diamondsuit \rightarrow nBA + \blacklozenge + \diamondsuit$	hydrogenation of the 1-butyl radical
10	$C_4^{II}H_9\blacklozenge + H\diamondsuit \rightarrow nBA + \blacklozenge + \diamondsuit$	hydrogenation of the 2-butyl radical

Table 4. Kinetic Expressions for the Overall Reactions

$$r_1 = \frac{k_1^{I} K_{1BE}^{ad} y_{1BE}}{DEN_{HC} DEN_{H_2}} f_h^{I}(H_2) + \frac{k_1^{II} K_{1BE}^{ad} y_{1BE}}{DEN_{HC} DEN_{H_2}} f_h^{II}(H_2)$$

$$r_2 = \frac{k_2 K_{cBE}^{ad} y_{cBE}}{DEN_{HC} DEN_{H_2}} f_h^{II}(H_2)$$

$$r_3 = \frac{k_3 K_{tBE}^{ad} y_{tBE}}{DEN_{HC} DEN_{H_2}} f_h^{II}(H_2)$$

$$r_4 = \frac{k_4 K_{1BE}^{ad}}{DEN_{HC} DEN_{H_2}} f_i^{II}(H_2)\left(y_{1BE} - \frac{y_{cBE}}{K_4^{eq}}\right)$$

$$r_5 = \frac{k_5 K_{1BE}^{ad}}{DEN_{HC} DEN_{H_2}} f_i^{II}(H_2)\left(y_{1BE} - \frac{y_{tBE}}{K_5^{eq}}\right)$$

$$r_6 = \frac{k_6 K_{cBE}^{ad}}{DEN_{HC} DEN_{H_2}} f_i^{II}(H_2)\left(y_{cBE} - \frac{y_{tBE}}{K_6^{eq}}\right)$$

$$DEN_{HC} = 1 + K_{1BE}^{ad} y_{1BE} + K_{cBE}^{ad} y_{cBE} + K_{tBE}^{ad} y_{tBE}$$

model A

$$DEN_{H_2} = 1 + K_{H_2}^{ad} y_{H_2}$$

$$f_h^{I}(H_2) = f_h^{II}(H_2) = f_i^{II}(H_2) = y_{H_2}$$

model D

$$DEN_{H_2} = 1 + \sqrt{K_{H_2}^{ad} y_{H_2}}$$

$$f_h^{I}(H_2) = \frac{y_{H_2}}{1 + \alpha\sqrt{K_{H_2}^{ad} y_{H_2}}}$$

$$f_h^{II}(H_2) = \frac{y_{H_2}}{1 + \beta\sqrt{y_{H_2}}}$$

$$f_i^{II}(H_2) = \frac{\sqrt{y_{H_2}}}{1 + \beta\sqrt{y_{H_2}}}$$

hydrogenation of $C_4^{I}H_9\blacklozenge$ and $C_4^{II}H_9\blacklozenge$, just as in steps 9 and 10 of Table 3.

Kinetic Expressions. To derive the overall kinetic expressions from the elementary steps of mechanism D, we assume that all adsorption steps, 1−4 in Table 3, are fast enough to remain equilibrated. We also assume that the fractions of sites of type ◆ occupied by butyl radicals and by *n*-butane are negligible. The same assumptions are made for mechanism A. In the case of model A, we additionally assume that the amount of sites of type ◇ covered by the intermediate H◇ is negligible.

The rate equations thus derived for the set of overall reactions in Figure 2, from either mechanism D or mechanism A, are listed in Table 4. The procedure followed to derive the rate equations was detailed by Bressa.[7]

The following features are common in both sets of kinetic expressions, which are denoted A and D in accordance with the corresponding mechanisms. The driving forces and the hydrocarbon adsorption term, DEN_{HC}, are linear with respect to the mole fractions of each hydrocarbon compound. As a result of the hypothesis of noncompetitive adsorption between H_2 and hydrocarbons, the adsorption term corresponding to H_2, DEN_{H_2}, is independent of that corresponding to hydrocarbons. Regarding all of these attributes, our kinetic expressions coincide with those derived by others.[4,6,9]

As mechanisms A and D differ only in the type of H_2 adsorption, the differences between the two sets of kinetic expressions lie in the dependence on the H_2 concentration.

Table 4 shows that the dependence on the H_2 concentration is the same in all reaction rate expressions from mechanism A. The driving forces and DEN_{H_2} are all first-order in H_2. Other authors have also employed first-order functions of the H_2 concentration to quantify the hydrogenation of *n*-butenes on Pd.[4,9] As a consequence of the undiscriminated effect of H_2, only the sum $(k_1^{I} + k_1^{II})$ in the rate expression for 1-butene hydrogenation, r_1, can be estimated from experimental data.

In the case of model D, DEN_{H_2} depends on the square root of y_{H_2}. The factor f_h^{I} in rate expression r_1 arises from *n*-butane formation through the route involving the radical $C_4^{I}H_9\blacklozenge$. The factor f_h^{II} in rate expressions r_1, r_2, and r_3 arises from *n*-butane formation through the route involving $C_4^{II}H_9\blacklozenge$. Both factors, f_h^{I} and f_h^{II}, can behave at most as first-order terms if the coefficients α and β are low. Instead, all isomerization reactions contain the factor f_i^{II} that, at most, can behave as a one-half-order term.

The overall kinetic coefficients in Table 4 can be written in terms of the kinetic coefficients of the elementary steps.[7] From these relationships, it is possible to conclude that not all of the overall coef-

ficients can take independent values. The following constraint is valid for both models

$$k_3 = \frac{k_2 k_5}{k_4} \frac{K_{cBE}^{ad}/K_{tBE}^{ad}}{K_6^{eq}} \quad (1)$$

In addition, the parameters k_1^{II} and β in model D can be expressed as

$$k_1^{II} = \frac{k_2 k_5}{k_6} \quad (2)$$

and

$$\beta = \frac{k_2 K_{cBE}^{ad}}{k_6 K_{cBE}^{ad}\left(1 + \frac{k_4}{k_5}\right) + \frac{k_4 K_{1BE}^{ad}}{K_4^{eq}}} \quad (3)$$

Highlights of the Kinetic Models. An examination of the kinetic expressions displayed in Table 4 will reveal whether they are able to capture the most significant trends exhibited by experimental data.

If the concentration of 1-butene is high enough to saturate sites of type ◆, then the product $K_{1BE}^{ad} y_{1BE}$ will be the only significant term in DEN_{HC}. Hence, 1-butene reactions will be zeroth-order in 1-butene, in accordance with the experimental results.

It is worth analyzing the features of the kinetic expressions that result if direct competition between H_2 and hydrocarbons for the same type of active sites as suggested in the literature[10] is considered. The driving forces remain as in Table 4, but the product $DEN_{HC}DEN_{H_2}$ in models A and D becomes

$$DEN_{HC}DEN_{H_2} = (1 + K_{1BE}^{ad} y_{1BE} + K_{cBE}^{ad} y_{cBE} + K_{tBE}^{ad} y_{tBE} + K_{H_2}^{ad} y_{H_2})^2 \quad (4)$$

and

$$DEN_{HC}DEN_{H_2} = (1 + K_{1BE}^{ad} y_{1BE} + K_{cBE}^{ad} y_{cBE} + K_{tBE}^{ad} y_{tBE} + \sqrt{K_{H_2}^{ad} y_{H_2}})^2 \quad (5)$$

respectively. These inhibition functions lead to negative orders of 1-butene if its concentration is high enough. However, the experimental results do not sustain this behavior.

Bond and Wells[2] predicted that the relative yield of *trans*- to *cis*-2-butene from the isomerization of 1-butene through the 2-butyl radical should be 1.85 and 1.2 at 0 and 150 °C, respectively. Our experimental results show that the trans/cis ratio lies between 2 and 1.5 for temperatures between −8 and 30 °C. This finding prompted us to propose that the isomerization reactions proceed through the 2-butyl radical.

Data Analysis

To simulate the experiments from the proposed kinetic models, the conservation mass balances along the catalyst bed should be solved. Plug flow was assumed, and isothermal and isobaric conditions were verified for all experimental settings. The routine DDASAC[16] was employed to obtain the numerical solution. (The code DDASAC has been superseded by the code DDAPLUS described at http://www.athenavisual.com and available from Stewart and Associates Engineering Software, Inc.)

According to Weisz's[18] criterion applied to the experimental data, intraparticle mass-transport limitations cannot be ruled out. Thus, effective reaction rates should be evaluated by integration over a representative particle for each cross section of the bed. Standard conservation equations were formulated within the active layer of the catalyst and solved[7] by the orthogonal collocation method. The tortuosity factor of the porous catalyst that arises from the internal diffusion model was regarded as an additional fitting parameter.

Intraparticle temperature gradients proved to be negligible because of the very low concentration of 1-butene, and as stated above, external limitations could be safely ignored.

Starting from initial guesses for the set of parameters, i.e., the kinetic parameters of either model A or model D and the tortuosity factor, the optimal values were computed by minimizing an adequate measure of the difference between the outlet composition predicted by the model and the experimental observations. In the case of the experimental results reported here, no data are missing in the matrix of observations, experimental errors are interdependent and the covariance matrix is unknown. For these conditions, the suitable criterion for parameter estimation is[19]

$$\min_{\theta} |Y| \quad (6)$$

where θ represents the vector of parameters; $|Y|$ is the determinant of the matrix of residuals $y_{j,n}^{exit}$ and $y_{k,n}^{exit}$ are

$$Y_{j,k} = \sum_n (y_{j,n}^{exit} - \hat{y}_{j,n})(y_{k,n}^{exit} - \hat{y}_{k,n}) \quad (7)$$

the measured mole fractions of hydrocarbons j and k, respectively, in experiment n; and $\hat{y}_{j,n}$ and $\hat{y}_{k,n}$ are their estimates predicted by the model.

We recall that the observed variables are the mole fractions of the four hydrocarbons. To solve the minimization problem posed in eq 6, we employed the code GREG[17] (which has been superseded by the code GREGPLUS described at http://www.athenavisual.com and available from Stewart and Associates Engineering Software, Inc.).

Results from the Regression Analysis

Model Discrimination. First, we analyze the experimental data obtained at −8 °C, as this set of observations yielded significant results about model discrimination.

Parameter estimates, i.e., modal values and inference intervals, can be useful criteria to use for rejecting models. In accordance with their physicochemical meanings, the modal values of the parameter estimates were all positive for both models. Thus, on this basis, neither of the models could be rejected.

Stewart et al.[20] recommended posterior probability as a natural criterion for model discrimination among rival candidates on the basis of multiresponse data.

Accordingly, the posterior probability share held by model D is

$$\pi_D = \frac{|\hat{Y}_D|^{-\nu_e/2}}{|\hat{Y}_D|^{-\nu_e/2} + |\hat{Y}_A|^{-\nu_e/2}} \quad (8)$$

where $\hat{Y}_m = Y_m(\hat{\theta}_m)$, $\hat{\theta}_m$ is the optimal vector of parameters for model m, m represents model D or A, and ν_e is the total number of replicate events minus the number of distinct settings at which replicates were done.

The result is overwhelmingly in favor of model D, as π_D exceeds 99.99%.

A comparison of the average relative error from the two models is also useful for model discrimination. The average relative error is defined as

$$\mathscr{R} = \frac{1}{R}\sum_{r=1}^{R}\left(\frac{1}{N}\sum_{n=1}^{N}\left|\mathscr{R}_{j,n}\right|\right) \quad (9)$$

where $\mathscr{R}_{j,n}$ stands for the residual deviation of compound j in experiment n

$$\mathscr{R}_{j,n} = 100\frac{\hat{y}_{j,n} - y_{j,n}^{exit}}{y_{j,n}^{exit}} \quad (10)$$

$R = 4$ is the number of responses, and $N = 70$ is the number of experiments at −8 °C.

The values of $\mathscr{R}$ are acceptably low, 11.15% for model A and 7.17% for model D. However, the precision of model D is 50% higher than that of model A. An analysis of some individual deviations $\mathscr{R}_{j,n}$ should reveal the causes for model D yielding a significantly better description of the experimental data.

Recalling that the main difference between the proposed kinetic models lies in the dependence of the reaction rates on the H_2 concentration, the experiments performed by varying the mole fraction of H_2 in the feed provide the most relevant information for model discrimination. Figure 7 illustrates the residual deviations of the 2-butenes and *n*-butane against the input H_2 content up to $y_{H_2}^{inlet} = 10\%$. For these data, $\mathscr{R}$ is significantly greater for model A than for model D, being 24.06 and 8.33%, respectively. At low values of $y_{H_2}^{inlet}$, model A grossly underestimates the 2-butenes and *n*-butane mole fractions, resulting in a noticeable systematic deviation, whereas deviations from model D are evenly distributed.

The better fit obtained with model D is due to the dependence of the driving force of the hydroisomerization reactions on $\sqrt{y_{H_2}}$. As explained in the next section, in practice, the driving force for 1-butene hydrogenation through the 1-butyl radical also becomes proportional to $\sqrt{y_{H_2}}$. Hence, the derivatives of these rate equations with respect to y_{H_2} are proportional to $1/\sqrt{y_{H_2}}$ and tend to high values as y_{H_2} decreases. This feature allows model D to provide a closer fit to the experimental data.

The inherent difficulty of model A in representing the experimental data in the lower range of H_2 forces some of its parameters to take values that are not the most appropriated for other experimental conditions. This is illustrated in Figure 8, where the results covering the whole range of 1-butene inlet mole fractions are presented. The deviations for model A show a significant

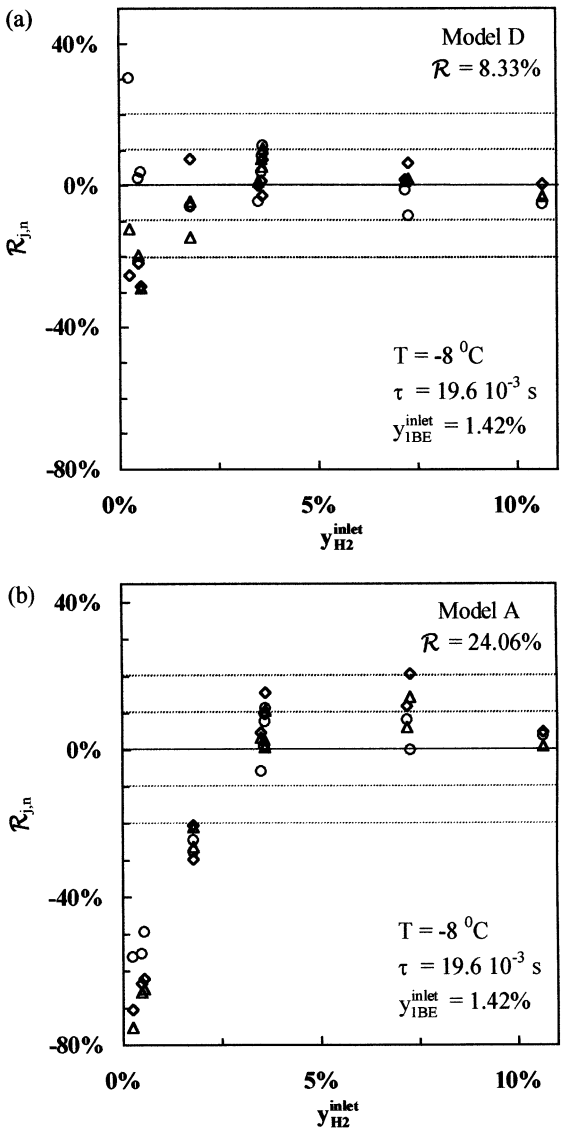

Figure 7. Residual deviations of the 2-butenes and *n*-butane against the settings of H_2 input at −8 °C: ◇, *cis*-2-butene; △, *trans*-2-butene; and ○, *n*-butane.

degree of correlation with y_{1BE}^{inlet}, whereas those for model D are again evenly distributed.

For the aforementioned reasons, the precision of the parameter estimates also becomes affected, as the inference intervals are in the range ±10−60% for model A compared to ±30% for model D.

The experimental results obtained for the remaining temperature levels, between 0 and 30 °C, were also considered for model discrimination. The values of $\mathscr{R}$ corresponding to the complete database between −8 and 30 °C, which includes 120 sets of operating conditions, are 12.55 and 8.84% for models A and D, respectively.

On the basis of the whole body of evidence, it can be safely concluded that model D is the best alternative between the two rival models proposed here.

Analysis of the Selected Model. *Estimates of the Kinetic Parameters.* The regression analysis was carried out in two steps. First, the data at −8 °C were analyzed to estimate the optimal parameter values at this temperature. Leaving these values fixed, because the widest range of composition was covered at −8 °C, the remaining sets of data were used to estimate the temperature dependence of the parameters according

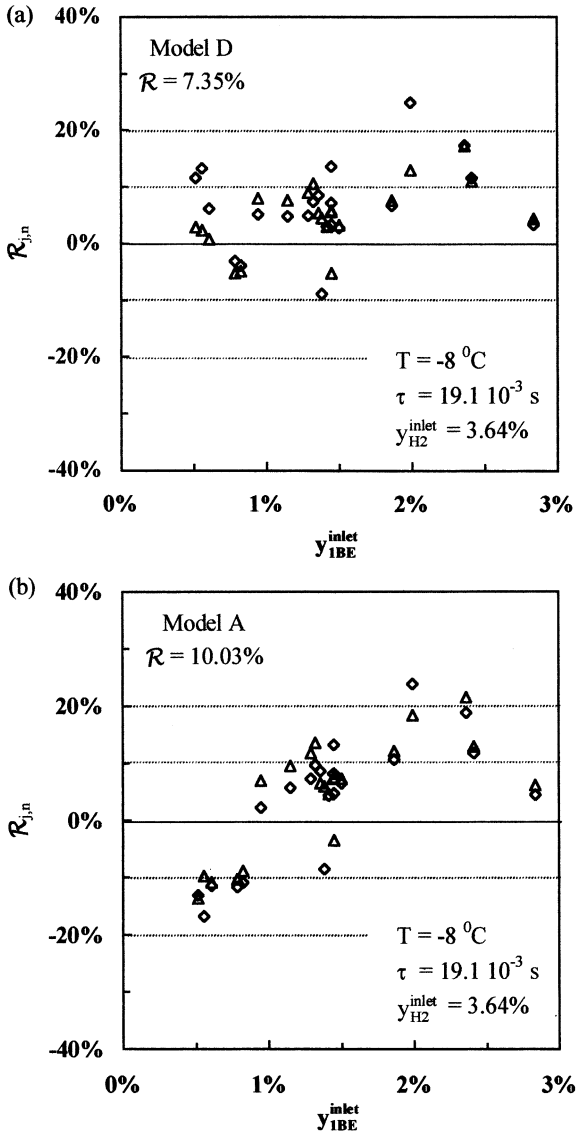

Figure 8. Residual deviations of the 2-butenes against the settings of 1-butene input at −8 °C: ◇, *cis*-2-butene and △, *trans*-2-butene.

to the relations

$$k(T) = k(T_{ref}) \exp\left[-\frac{E}{R}\left(\frac{1}{T} - \frac{1}{T_{ref}}\right)\right] \qquad (11)$$

and

$$K^{ad}(T) = K^{ad}(T_{ref}) \exp\left[-\frac{\Delta H^{ad}}{R}\left(\frac{1}{T} - \frac{1}{T_{ref}}\right)\right] \qquad (12)$$

where E is the activation energy, ΔH^{ad} is the adsorption enthalpy, R is the ideal gas law constant, T is the temperature, and T_{ref} is 265 K (−8 °C). This type of expression is recommended to avoid a strong correlation between the Arrhenius constants (see, e.g., Box[21]).

The modal values of the parameters and their 95% inference intervals are reported in Table 5.

It was impossible to estimate reliable individual values of the 2-butene adsorption constants. Thus, these values were replaced by an overall term of $K_{2BE}^{ad}(y_{cBE} + y_{tBE})$ in DEN_{HC}. Even so, Table 5 shows that the estimate of K_{2BE}^{ad} presents a large inference interval. Additional experiments with higher 2-butenes concentrations would enhance the precision of K_{2BE}^{ad}. According to expectations from the estimate of K_{2BE}^{ad} at −8 °C, the value of ΔH_{2BE}^{ad} was not statistically significant.

An unacceptable inference interval was also obtained for $\Delta H_{H_2}^{ad}$. The modal value of $K_{H_2}^{ad}$ at −8 °C is rather low, and it should decrease with temperature. For this reason, we concluded that the H_2 mole fraction levels were not high enough to assess the inhibition effect of H_2 at high temperature.

The parameter α in the term f_h^I (cf. Table 4) relates the elementary kinetic coefficient corresponding to the hydrogenation of $C_4^IH_9◆$, step 9 in Table 3, to that of the dehydrogenation of $C_4^IH_9◆$ to 1-butene, step 5. Preliminary regression analysis gave high values of α. This result suggests that the addition of the second hydrogen atom to $C_4^IH_9◆$ is very fast, as was assumed by Goetz et al.[6]

Because of the high value of α, k_1^I and α were strongly correlated. Therefore, the hydrogenation rate of 1-butene through the 1-butyl radical was finally expressed as

$$r_1^I = \frac{k_1 K_{1BE}^{ad} y_{1BE} \sqrt{y_{H_2}}}{DEN_{HC} DEN_{H_2}} \qquad (13)$$

where $k_1 = k_1^I/(\alpha\sqrt{K_{H_2}^{ad}})$.

The modal values of the adsorption constants at −8 °C indicate large differences between the individual adsorption strengths, in the sequence 1-butene ≫ 2-butenes ≫ H_2.

The five kinetic coefficients independently estimated were k_1, k_2, k_4, k_5, and k_6. The inference intervals listed in Table 5, about 35% for each of them, can be regarded as being satisfactory.

The dependent parameters k_3, k_1^{II}, and β, which were not included in θ but computed from eqs 1−3, are also given in Table 5. Some exploratory calculations in which k_3, k_1^{II}, and β were optimized as independent parameters were also made. The estimates thus obtained for k_1^{II} and β, $(9.919 \pm 3.993) \times 10^{-2}$ mol/($kg_{active\ shell}$ s) and $(4.053 \pm 0.978) \times 10^{-1}$, respectively, agree satisfactorily with those in Table 5. In the test in which k_3 was evaluated as an independent parameter, a strong correlation between k_3 and k_2 led to wide inference intervals for both parameters.

Table 5 shows that the inference intervals for the E_1−E_5 estimates are remarkably low. Also, ΔH_{1BE}^{ad} exhibits satisfactory precision. The low but uncertain value obtained for E_6 indicates that the influence of temperature on cis−trans isomerization is moderate. A temperature range wider than that employed in this work would be needed to determine its value with higher precision.

The results from solving the mass conservation equations inside the catalyst showed that the internal mass-transport resistance affected the effective reaction rates throughout the experimental range, but mainly at higher temperature. For instance, at 20 °C and $y_{H_2}^{inlet} >$ 3%, the effectiveness factor corresponding to the global rate of consumption of 1-butene, i.e., $r_1 + r_4 + r_5$, was somewhat lower than 0.4. The nonnegligible effect of

Table 5. Optimal Values of the Kinetic Parameters Corresponding to the Selected Model D

parameter estimates at −8 °C	
parameters evaluated by data fitting	dependent parameters
$k_1 = (1.832 \pm 0.661) \times 10^{-1}$ mol/(kg$_{\text{active shell}}$ s)	$k_1^{II} = \frac{k_2 k_5}{k_6} = 7.498 \times 10^{-2}$ mol/(kg$_{\text{active shell}}$ s)
$k_2 = (4.186 \pm 1.460) \times 10^{-1}$ mol/(g$_{\text{active shell}}$ s)	
$k_4 = (6.545 \pm 2.178) \times 10^{-2}$ mol/(kg$_{\text{active shell}}$ s)	$k_3 = \frac{k_2 k_5}{k_4 K_6^{eq}} = 1.655 \times 10^{-1}$ mol/(kg$_{\text{active shell}}$ s)
$k_5 = (1.036 \pm 0.346) \times 10^{-1}$ mol/(kg$_{\text{active shell}}$ s)	
$k_6 = (5.787 \pm 1.966) \times 10^{-1}$ mol/(kg$_{\text{active shell}}$ s)	
$K_{1BE}^{ad} = (5.676 \pm 2.070) \times 10^{2}$	$\beta = \frac{k_2 K_{2BE}^{ad}}{k_6 K_{2BE}^{ad}\left(1 + \frac{k_4}{k_5}\right) + \frac{k_4 K_{1BE}^{ad}}{K_4^{eq}}} = 4.110 \times 10^{-1}$
$K_{2BE}^{ad} = (4.049 \pm 6.684) \times 10^{1}$	
$K_{H_2}^{ad} = (2.417 \pm 0.570)$	
activation energy and adsorption enthalpy estimates	
$E_1 = (2.651 \pm 0.226) \times 10^{1}$ kJ/mol	$E_5 = (3.796 \pm 0.190) \times 10^{1}$ kJ/mol
$E_2 = (4.067 \pm 0.431) \times 10^{1}$ kJ/mol	$E_6 = (6.702 \pm 5.443)$ kJ/mol
$E_4 = (3.319 \pm 0.220) \times 10^{1}$ kJ/mol	$\Delta H_{1BE}^{ad} = -(1.679 \pm 0.557) \times 10^{1}$ kJ/mol

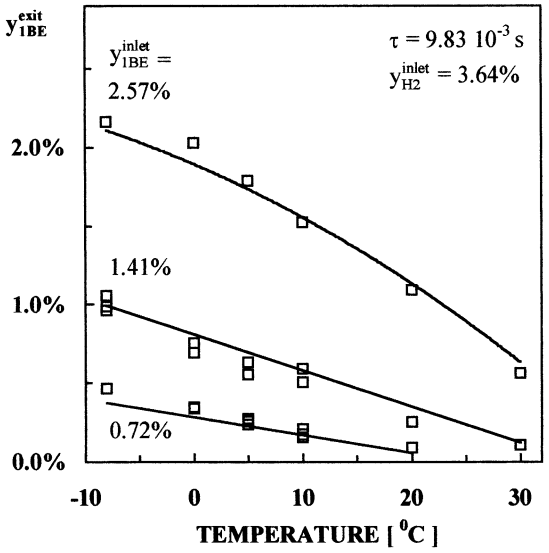

Figure 9. Exit 1-butene mole fraction as a function of 1-butene input and temperature.

mass-transport limitations allowed us to estimate the tortuosity factor as $\kappa = 1.516 \pm 0.631$.

The chemical equilibrium constants of the isomerization reactions were calculated at each temperature from thermodynamic data.

Data Fitting. Figures 3−6 exhibit comparisons between experimental data and model predictions. It can readily be seen that the selected model actually captures the observed behavior. Figures 9−12 extend the comparison to almost the complete range of operating conditions.

For the data in Figure 9, the 1-butene inhibition term covers a wide range of variation, from $K_{1BE}^{ad}\, y_{1BE}^{inlet} = 15$ at −8 °C to $K_{1BE}^{ad}\, y_{1BE}^{exit} = 0.2$ at 30 °C. Thus, the apparent 1-butene order of reaction varies from zeroth-order at low temperature and high 1-butene concentration to nearly first-order at high temperature and low 1-butene concentration. It can be observed that model D accurately predicts the experimental measurements along the whole range of settings in Figure 9.

The information plotted in Figures 10 and 11 was selected to compare the experimental production of 2-butenes and *n*-butane with the values predicted by the model. The comparison extends over the whole range of temperature at two levels of each space-time and H_2 input.

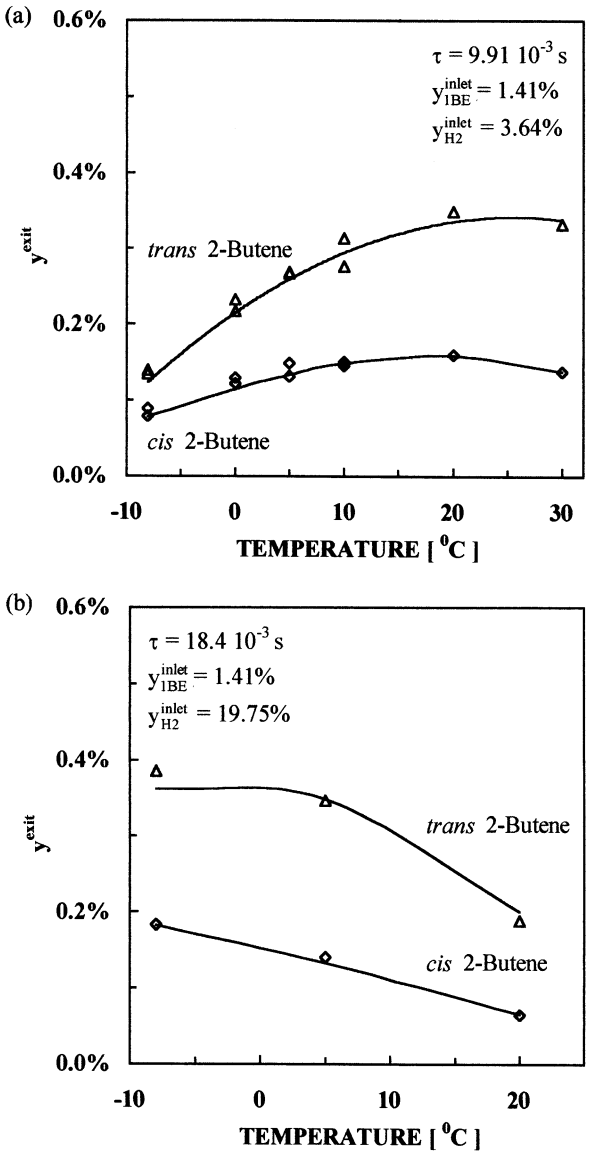

Figure 10. 2-Butenes production as a function of temperature for (a) low and (b) high levels of space-time and H_2 input.

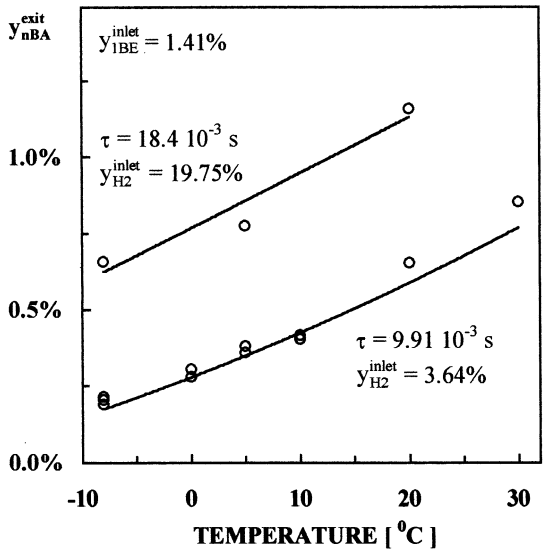

Figure 11. *n*-Butane production as a function of temperature for high and low levels of space-time and H_2 input.

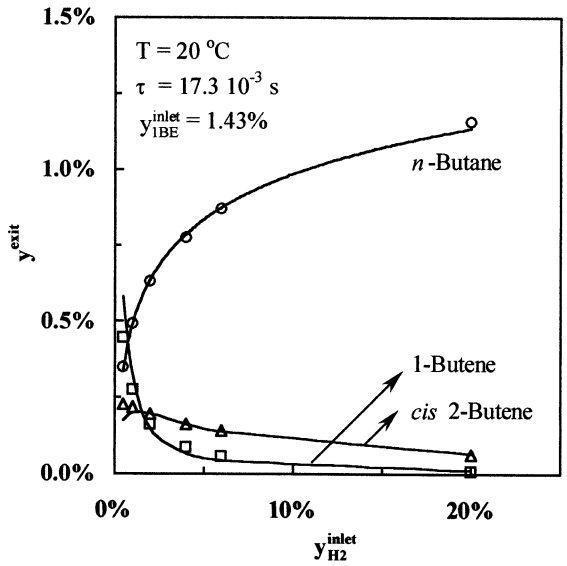

Figure 12. Variation of the exit composition with H_2 input at 20 °C.

The effect of temperature on the production of the 2-butenes can be assessed from Figure 10. In Figure 10b, at the high levels of τ and $y^{inlet}_{H_2}$, the rate of hydrogenation of 2-butenes is high enough to render a neat decreasing trend with temperature. In accordance with Figure 10, the *n*-butane production shown in Figure 11 increases with temperature. We conclude from Figures 10 and 11 that the model is satisfactorily precise in describing the experimental product distribution over the whole range of operating conditions.

The experiments performed at −8 °C at different H_2 concentrations were decisive for model discrimination. Thus, it is important to highlight that model D is able to accurately describe the effect of $y^{inlet}_{H_2}$ on the exit composition at higher temperatures, as shown in Figure 12 for data measured at 20 °C.

Comparison with Background Information

Although a complete set of kinetic parameters for the system of reactions studied in this paper is not available in the literature, results for a variety of operating conditions and catalysts providing partial kinetic information are available. Hence, some published results can be used here for a comparison with our results.

Table 5 shows that $K^{ad}_{1BE} \gg K^{ad}_{2BE} \gg K^{ad}_{H_2}$. This ranking confirms experimental trends found by other authors.[4,22]

Boitiaux et al.[4] and Kiperman[14] reported values of activation energies for the hydrogenation and hydroisomerization of *n*-butenes over Pd in the range of 38−42 kJ/mol or rather lower. These values agree with our estimates that, considering the inference intervals in Table 5, range between 27 and 41 kJ/mol.

Kripylo et al.[9] studied the hydrogenation of 1,3-butadiene over a commercial Pd catalyst. From their experiments, performed between 60 and 140 °C, a unique value of the adsorption enthalpy for the three *n*-butenes was estimated: $\Delta H^{ad}_{nBE} = -15$ kJ/mol. This value compares well with the modal value for the 1-butene adsorption enthalpy in Table 5: $\Delta H^{ad}_{1BE} = -16.79$ kJ/mol.

Hub et al.[23] calculated the turnover number (TON) for the overall consumption of 1-butene. They employed a Pd/Al_2O_3 catalyst containing 0.45 wt % Pd with 26% dispersion. Vapor-phase experiments at atmospheric pressure and 0 °C evidenced zeroth-order behavior in 1-butene. For a H_2 mole fraction of 5%, the TON was 4 s^{-1}. The intrinsic TON predicted by our model under the same operating conditions is 5.7 s^{-1}. We conclude that the two catalysts show similar activity levels under the same experimental conditions.

The models posed by Zhang and Seaton[24] and by Weisberg[25] were used to evaluate the tortuosity factor, κ, from pore structure features of the catalyst employed in this study. These models predict $\kappa = 1.5$ and 1.4, respectively. The modal value of the tortuosity factor obtained by data fitting, $\kappa = 1.52$, is in complete agreement with the values obtained from pore structure characteristics.

Conclusions

The vapor-phase hydrogenation and hydroisomerization of the *n*-butenes on a Pd-based commercial catalyst of the eggshell type was investigated at six temperatures between −8 and 30 °C; at atmospheric pressure; for space-times ranging from 5×10^{-3} to 55×10^{-3} s^{-1}; and for 1-butene and H_2 inputs up to 3 and 50%, respectively.

We proposed two sets of rate equations to represent the experimental behavior. These proposals were derived from mechanisms based on dissociative and associative adsorption of H_2, models D and A, respectively. Hence, the rival sets of rate equations essentially differed only in their dependence on the H_2 concentration. In the case of model D, the driving forces for the hydrogenation and hydroisomerization reactions turned out to be first-order and one-half-order in H_2, respectively, whereas model A predicts a first-order dependence for all reactions.

Although both models satisfactorily represent the experimental results, model D is significantly more accurate, and unlike model A, it yields uniform residual deviations throughout the range of operating conditions investigated.

The relative average deviation from model D, over all hydrocarbon species and 120 sets of experimental conditions, is 8.84%. The complete set of kinetic coefficients and the H_2 and 1-butene adsorption constants were reliably estimated from data measured at −8 °C. The

adsorption constants of the 2-butenes were poorly determined because their inhibition effects were not relevant in describing the available data. The experimental data between 0 and 30 °C allowed us to obtain precise values of the 1-butene adsorption enthalpy and activation energies, except for the cis−trans isomerization. Additional experiments at lower temperatures and higher H_2 concentrations would be necessary to evaluate the adsorption enthalpy of hydrogen.

The very fast *n*-butenes reactions on Pd led to significant internal concentration gradients. Therefore, the mass conservation equations inside the catalyst had to be solved to evaluate the intrinsic values of kinetic parameters. The catalyst tortuosity factor was introduced as a fitting parameter. The fact that the estimated value of the tortuosity factor agrees well with values predicted from the characteristics of the catalyst structure indicates that the role of diffusion was correctly assessed.

Acknowledgment

We thank ANPCyT (PICT 14-06297, P.BID 1201/OC-AR), CONICET (PIP96 4791) and UNLP (PI 1078) for their financial assistance. OMM and GFB are members of Consejo Nacional de Investigaciones Científicas y Técnicas. SPB is member of Comisión de Investigaciones Científicas de la Provincia de Buenos Aires.

Nomenclature

E_i = activation energy corresponding to the overall reaction i, kJ/mol
ΔH_j^{ad} = adsorption enthalpy of compound j, kJ/mol
K_j^{ad} = adsorption constant of compound j
k_i = kinetic coefficient corresponding to the overall reaction i, mol/($kg_{active\ shell}$ s)
R = ideal gas law constant, 8.314 J/(mol K)
$\mathscr{R}$ = average relative error defined in eq 9
$\mathscr{R}_{j,n}$ = residual deviation of hydrocarbon j in experiment n, defined in eq 10
r_i = reaction rate corresponding to the overall reaction i, mol/($kg_{active\ shell}$ s)
y_j = mole fraction of compound j inside the active shell
$\hat{y}_j$ = mole fraction of hydrocarbon j predicted by the model
y_j^{exit} = exit mole fraction of compound j
y_j^{inlet} = mole fraction of compound j in the feed

Greek Symbols

κ = tortuosity factor
ν_e = number of error degrees of freedom in the replicate comparisons
π_D = probability share held by model D defined in eq 8
θ = vector of parameters that are to be evaluated by data fitting
τ = space-time, s
Y = matrix of residuals defined in eq 7

Subscripts

1BE = 1-butene
cBE = *cis*-2-butene
tBE = *trans*-2-butene
*n*BA = *n*-butane
2BE = 2-butenes
H_2 = hydrogen

Literature Cited

(1) Derrien, M. L. Selective Hydrogenation Applied to the Refining of Petrochemical Raw Materials Produced by Steam Cracking. *Stud. Surf. Sci. Catal.* **1986**, *27*, 613.

(2) Bond, G. C.; Wells, P. B. The Mechanism of the Hydrogenation of Unsaturated Hydrocarbons on Transition Metal Catalysts. *Adv. Catal.* **1963**, *15*, 91.

(3) Webb, G. Hydrogenation of Alkenes and Alkynes and Related Reactions Catalysed by Metals and Metal Complexes. *Catalysis* **1980**, *4*, 145.

(4) Boitiaux, J. P.; Cosyns, J.; Derrien, M. L.; Leger, G. Proper Design of Butadiene Selective Hydrogenation Process for Maximum 1-Butene Yield by Using Comprehensive Kinetic Modelling. In *Proceedings of the AIChE Spring National Meeting*; American Institute of Chemical Engineers (AIChE): New York, 1985; Paper 1453.

(5) Vergel, C.; Euzen, J. P.; Trambouze, P.; Wauquier, J. P. Two-Phase Flow Catalytic Reactor, Influence of Hydrodynamics on Selectivity. *Chem. Eng. Sci.* **1995**, *50*, 3303.

(6) Goetz, J.; Touroude, R.; Murzin, D. Y. Kinetics of Buta-1,3-diene Hydrogenation over 0.5% Pd/γ-Al_2O_3 Catalust. *Chem. Eng. Technol.* **1997**, *20*, 138.

(7) Bressa, S. P. Purificación Catalítica de 1-Buteno: Estudio Cinético y Simulación de un Reactor Industrial de Hidrogenación Selectiva. Ph.D. Thesis, Universidad Nacional de La Plata, La Plata, Argentina, 2001.

(8) van den Bleek, C. M.; van der Wiele, K.; van den Berg, P. J. The Effect of Dilution on the Degree of Conversion in Fixed Bed Catalytic Reactors. *Chem. Eng. Sci.* **1969**, *24*, 681.

(9) Kripylo, P.; Turek, F.; Hempe, K.-D.; Kirmse, H. Kinetics and Mechanisms of the Hydrogenation of 1,3-Dienes over Pd Catalysts. Part II. *Chem. Technol.* **1975**, *27*, 675.

(10) Boitiaux, J. P.; Cosyns, J.; Robert, E. Liquid Phase Hydrogenation of Unsaturated Hydrocarbons on Palladium, Platinum and Rhodium Catalysts. Part I: Kinetic Study of 1-Butene, 1,3-Butadiene and 1-Butyne Hydrogenation on Platinum. *Appl. Catal.* **1987**, *32*, 145.

(11) Boitiaux, J. P.; Cosyns, J.; Robert, E. Hydrogenation of Unsaturated Hydrocarbons in Liquid Phase on Palladium, Platinum and Rhodium Catalysts. Part III: Quantitative Selectivity Ranking of Platinum, Palladium and Rhodium in the Hydrogenation of 1-Butene, 1,3-Butadiene and 1-Butyne Using a Single Reaction Scheme. *Appl. Catal.* **1987**, *35*, 193.

(12) Ouchaib, T.; Massardier, J.; Renouprez, A. Competitive Hydrogenation of Butadiene and Butene on Palladium and Platinum Catalysts. *J. Catal.* **1989**, *119*, 517.

(13) Bos, A. N. R.; Westerterp, K. R. Mechanism and Kinetics of the Selective Hydrogenation of Ethyne and Ethene. *Chem. Eng. Process.* **1993**, *32*, 1.

(14) Kiperman, S. L. Some Problems of Chemical Kinetics in Heterogeneous Hydrogenation Catalysis. *Stud. Surf. Sci.* **1986**, *27*, 1.

(15) Uygur, H.; Atalay, S.; Savaşçi, T. Kinetics of Liquid Phase Selective Hydrogenation of Methylacetylene and Propadiene in C_3 Streams. *J. Chem. Eng. Jpn.* **1998**, *31*, 178.

(16) Caracotsios, M.; Stewart, W. E. Sensitivity Analysis of Initial Value Problems with Mixed ODEs and Algebraic Equations. *Comput. Chem. Eng.* **1985**, *9*, 359.

(17) Stewart, W. E.; Caracotsios, M.; Sørensen, J. P. Parameter Estimation from Multiresponse Data. *AIChE J.* **1992**, *38*, 641.

(18) Weisz, P. B.; Hicks, J. S. The Behaviour of Porous Catalysts Particles in View of Internal Mass and Heat Diffusion Effects. *Chem. Eng. Sci.* **1962**, *17*, 265.

(19) Box, G. E. P.; Draper, N. R. The Bayesian Estimation of Common Parameters from Several Responses. *Biometrika* **1965**, *52*, 355.

(20) Stewart, W. E.; Shon, Y.; Box, G. E. P. Discrimination and Goodness of Fit of Multiresponse Mechanistic Models. *AIChE J.* **1998**, *44*, 1404.

(21) Box, G. E. P. Fitting Empirical Data. *Ann. N.Y. Acad. Sci.* **1960**, *86*, 792.

(22) Bond, G. C.; Webb, G.; Wells, P. B.; Winterbottom, J. M. The Hydrogenation of Alkadienes. Part I. The Hydrogenation of

Buta-1,3-diene Catalysed by the Noble Group VIII Metals. *J. Chem. Soc.* **1965**, 3218.

(23) Hub, S.; Hilaire, L.; Touroude, R. Hydrogenation of 1-Butyne and But-1-ene on Palladium Catalysts. *Appl. Catal.* **1988**, *36*, 307.

(24) Zhang, L.; Seaton, N. A. Prediction of the Effective Diffusivity in Pore Networks Close to a Percolation Threshold. *AIChE J.* **1992**, *38*, 1816.

(25) Whitaker, S. *The Method of Volume Averaging*; Kluwer Academic Publishers: Dordrecht, The Netherlands, 1999.

Received for review December 9, 2002
Revised manuscript received March 4, 2003
Accepted March 6, 2003

IE0209879